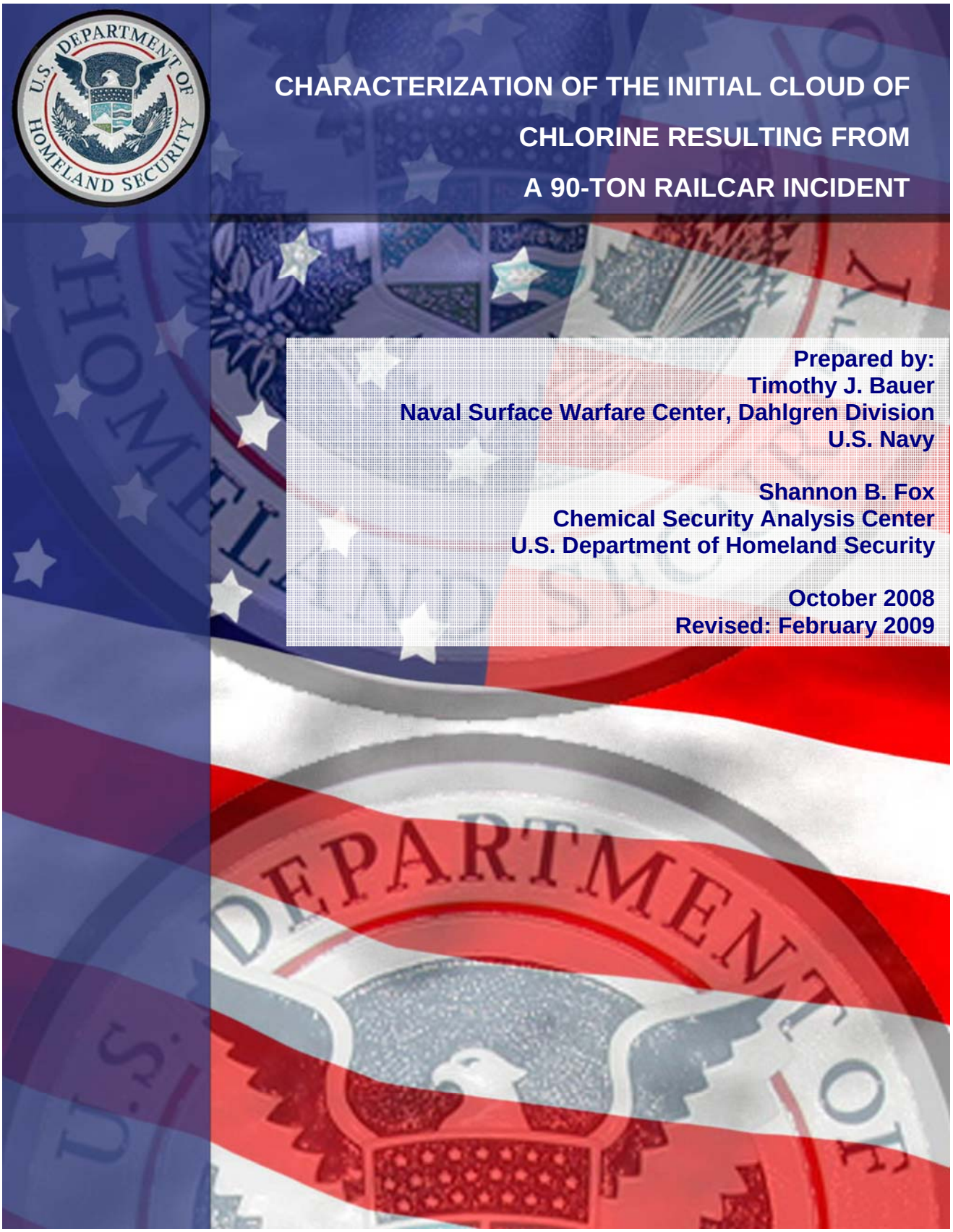

CHARACTERIZATION OF THE INITIAL CLOUD OF CHLORINE RESULTING FROM A 90-TON RAILCAR INCIDENT

Prepared by:
Timothy J. Bauer
Naval Surface Warfare Center, Dahlgren Division
U.S. Navy

Shannon B. Fox
Chemical Security Analysis Center
U.S. Department of Homeland Security

October 2008
Revised: February 2009

This page intentionally left blank.

Homeland Security

Chemical Security Analysis Center

Department Of Homeland Security

CHARACTERIZATION OF THE INITIAL CLOUD OF CHLORINE RESULTING FROM A 90-TON RAILCAR INCIDENT

Prepared by:
Timothy J. Bauer
U.S. Navy
Naval Surface Warfare Center, Dahlgren Division
Dahlgren, VA 22448-5162

Shannon B. Fox
U.S. Department of Homeland Security
Chemical Security Analysis Center
Aberdeen Proving Ground, MD 21010-5424

October 2008
Revised: February 2009

Acknowledgements

The authors wish to thank the Transportation Security Administration for funding the analytical work resulting in this paper. The authors also thank the following offices and individuals for providing input and technical feedback on the mist pool theory and the content of this paper: Chemical Security Analysis Center (CSAC), Stephen Chester of Battelle Memorial Institute, Curtis Schuhmacher of Northrop Grumman, Steven Hanna of Hanna Consultants, Joseph Chang of the Homeland Security Institute, Dyron Hamlin of the Center for Toxicology and Environmental Health, David Bacon of Science Applications International Corporation, John Cockayne of the Armed Forces Medical Intelligence Center, the Naval Research Laboratory in Washington, DC, Tom Spicer of the University of Arkansas, Rex Britter of Cambridge Environmental Research Consultants, Gene Lee of Baker Engineering and Risk Consultants, and Olav Hansen of GexCon AS, and Dr. Chris Cramer of the University of Minnesota and Joe Urban of the United States Naval Academy for reviewing the report. Sharon Sharp of CSAC is also acknowledged for her assistance in editing and preparing the final report.

Disclaimer

REPORT DOCUMENTATION PAGE

Form Approved
OMB No. 0704-0188

1. AGENCY USE ONLY (Leave blank)	2. REPORT DATE	3. REPORT TYPE AND DATES COVERED
	10/03/2008 Revised 02/24/2009	Technical N/A

4. TITLE AND SUBTITLE

CHARACTERIZATION OF THE INITIAL CLOUD OF CHLORINE RESULTING FROM A 90-TON RAILCAR INCIDENT

5. FUNDING NUMBERS

N/A

6. AUTHOR(S)

Timothy J. Bauer, Naval Surface Warfare Center, Dahlgren Division

Shannon B. Fox, Chemical Security Analysis Center,
U.S. Department of Homeland Security

7. PERFORMING ORGANIZATION NAME(S) AND ADDRESS(ES)

US Army Edgewood Chemical Biological Center
5183 Blackhawk Road (ATTN: AMSRD-ECB-RT-IM)
Aberdeen Proving Ground, MD 21010-5424

8. PERFORMING ORGANIZATION REPORT NUMBER

N/A

9. SPONSORING/MONITORING AGENCY NAME(S) AND ADDRESS(ES)

Department of Homeland Security,
Chemical Security Analysis Center
5183 Blackhawk Road
Aberdeen Proving Ground, MD 21010-5424

10. SPONSORING/MONITORING AGENCY REPORT NUMBER

N/A

11. SUPPLEMENTARY NOTES

None

12A. DISTRIBUTION/AVAILABILITY STATEMENT

Approved for public release; distribution is unlimited.

12B. DISTRIBUTION CODE

N/A

13. ABSTRACT (Maximum 200 words)

There is concern amongst city planners, the chemical industry, the railway transportation industry, and the Transportation Security Administration about the consequences of a release from a railcar containing a large quantity of chlorine or other toxic industrial chemical while transiting near a city. Estimates using modern dense gas models suggest that tens of thousands of persons could become chlorine casualties. Conversely, recent railway accidents resulting in release of massive quantities of chlorine have resulted in few deaths and low numbers of persons requiring medical treatment. Hazard estimation experts have proposed three mechanisms that the models do not account for that would lead to many fewer predicted casualties: removal of chemical near the source by absorption into and reaction with surface materials, vegetation, water, and air; better interpretation of human toxicity values for inhalation exposure; and increased release duration at the source resulting in lower concentrations over a longer exposure period. This paper addresses the last of these mechanisms by proposing a physical process, referred to as a mist pool, which results in lower chemical concentrations downwind of the release location. The sequence of physical processes proceeding and including characterization of the mist pool is presented for an example incident.

14. SUBJECT TERMS	15. NUMBER OF PAGES
mist pool; dense gas; hazard estimation; toxic industrial chemical; chlorine; railcar	34
	16. PRICE CODE

17. SECURITY CLASSIFICATION OF REPORT	18. SECURITY CLASSIFICATION OF THIS PAGE	19. SECURITY CLASSIFICATION OF ABSTRACT	20. LIMITATION OF ABSTRACT
UNCLASSIFIED	UNCLASSIFIED	UNCLASSIFIED	UNLIMITED

NSN 7540-01-280-5500

Standard Form 298 (Rev. 2-89)
Prescribed by ANSI Std. 239-18
298-102

This page intentionally left blank.

TABLE OF CONTENTS

FIGURE

TABLES

This page intentionally left blank.

CHARACTERIZATION OF THE INITIAL CLOUD OF CHLORINE RESULTING FROM A 90-TON RAILCAR INCIDENT

1.0 INTRODUCTION

A release from a railcar containing chlorine or other toxic industrial chemical while transiting near a city is of great concern. There is currently disagreement between model predictions of the distance that the resulting toxic cloud of chlorine vapor travels at human exposure levels resulting in death or requiring medical treatment[1] and records of casualties following recent incidents.[2] This paper provides a mathematical analysis of the physical processes occurring following breach of a chlorine railcar through intentional or accidental means. The relevant toxic cloud formation processes following creation of a hole or rupture in the liquid space include tank equilibrium, jet velocity and flow rate, jet adiabatic expansion, air entrainment into the jet, and cloud equilibrium. At this point, modern dense gas hazard assessment models assume the jet is carried downwind with the passing air and continue to entrain air and its associated mass, momentum, and energy. In some models, dense gas slumping calculations precede the interaction with the wind.[3]

This paper proposes an additional process that occurs when the rate of chemical flow out of the tank exceeds the capacity of the passing air to carry it downwind. The chemical accumulates at the release location and forms a large, flat cloud of very dense aerosol and vapor called a mist pool. The mist pool interacts with the air above through entrainment of chemical into the air across the cloud top area. The mist pool behavior is compared to the normal jet behavior in Figure 1.

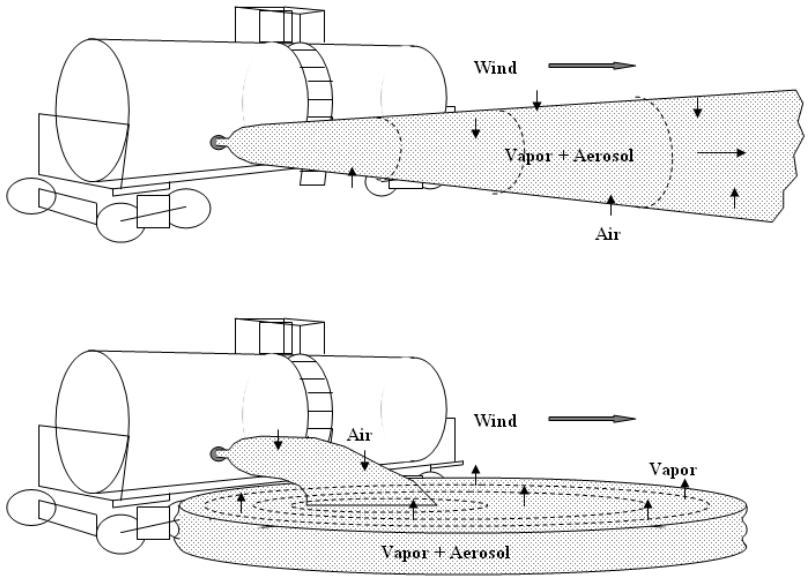

Figure 1. Cloud Formation for (a) normal jet taken up by the wind, and (b) mist pool.*

* The dashed lines show the progression of each type of release with time.

Normal transport and diffusion algorithms still apply to this vapor area flux. The result of mist pool formation is thus an area source of longer duration than the tank empty time leading to lower concentrations downwind. A criterion is proposed to determine when a mist pool will form. Attacks on railcars filled with chlorine and ammonia are used as examples to demonstrate the complete sequence of events.

2.0 THEORY

2.1 Attack and Tank Conditions

The processes addressed by the mist pool are relevant to industrial chemicals that are stored in multi-ton quantities as liquid under pressure and at temperatures above the chemical boiling point. Relevant chemicals include chlorine, anhydrous ammonia, liquefied natural gas, Freon, propane, and butane. Steam stored at temperatures below about 180 °C exhibits similar physical processes. The hole or rupture resulting from the attack is assumed to be well below the chlorine vapor-liquid interface, most likely about ⅓ of the way up from the tank bottom to the top. Breaches in the vapor space are not addressed. This paper will focus on chlorine railcar tanks, which are only transported full or empty. Ammonia stored in the same tank under similar conditions is considered for comparison purposes.

The tank cars are not refrigerated, but the 4-inch layer of insulation between the tank and the metal jacket results in a very slow temperature increase from the filling temperature to ambient temperature. The derivations and analysis here assume there has been sufficient time (e.g., several days) between filling and incident occurrence for the chlorine liquid to reach ambient temperature. The difference between the tank temperature and the liquid boiling temperature is defined as the temperature of superheating. The range of superheating considered is taken to be between 20 °C and 80 °C. Chlorine has a boiling point of -34 °C, and ammonia has a boiling point of -33 °C, so the relevant tank temperature range is between -13 °C and 46 °C. The characteristics of the jet passing through the hole change outside of this range. Lower superheating has been shown to result in significant rainout and pooling, while higher superheating can result in vapor forming while the liquid passes through the hole instead of after exposure to ambient pressure.

2.2 Tank Emptying Equilibrium

Although the formation of jet flow through the hole may be the first physical process to occur upon hole formation, the jet flow rate is a function of tank pressure and jet density, both of which vary as the tank empties. The following assumptions are made: 1) negligible heat transfer through the tank and insulation layers during the tank emptying process; 2) no air enters the tank until after it depressurizes to ambient pressure; and 3) there are no heat and mass transfer factors resulting in temperature differences between the liquid in the tank and the vapor in the head space. The behavior of the contents of the tank while it empties is thus treated strictly as an equilibrium process.

Observations by emergency responders from chlorine railcar incidents confirm that the contents of the tank auto-refrigerate leaving liquid and vapor inside the tank at ambient pressure of 101.325 kPa (1 atm) and the liquid boiling temperature. The final tank conditions are comprised of the remaining liquid mass plus the vapor in the head space, which is in equilibrium at the boiling temperature. This paper does not address processes within the tank subsequent to release of the tank contents and auto-refrigeration.

It is assumed that there is always liquid inside the hole until the vapor-liquid interface reaches the top of the hole. Under the attack conditions considered, it is expected that there is insufficient energy imparted to the tank contents to lead to foaming. The liquid head pressure is expected to prevent bubble formation at the hole position until the vapor-liquid interface gets very close to the top of the hole.[4] When the vapor phase is finally exposed to the atmosphere, the head space rapidly depressurizes from the equilibrium pressure to ambient pressure. It is during this depressurization that the auto-refrigeration occurs. Vapor is generated through flashing until the liquid and vapor in the tank cool to the boiling temperature. Unless the hole is a very long vertical gash, the time between the interface moving from the top of the hole to the bottom should be small compared to the overall tank empty time, so this intermediate phase is not considered.

Tank volume, V_{tank}, is estimated from initial mass, M_{tank}, and liquid density, $\rho_{L,tank}$:

$$V_{tank} = M_{tank} / \rho_{L,tank} \quad [1]$$

This volume is equal to the partial volumes of remaining liquid and head space vapor:

$$V_{tank} = M_R / \rho_L + M_{hs} / \rho_V \quad [2]$$

where ρ_V and ρ_L represents the vapor and liquid densities respectively at the boiling temperature. M_R and M_{hs} equal the recovered liquid mass and the head space vapor mass. Total toxic industrial chemical mass released, M_{TIC}, equals the combined liquid and vapor mass expelled from the tank:

$$M_{TIC} = M_{tank} - M_R - M_{hs} \quad [3]$$

Until the liquid empties to the top of the hole, the pressure remains at saturation for the tank temperature. As soon as the vapor space reaches the hole area, rapid depressurization with the associated auto-refrigeration begins. The tank conditions can be determined at this point just before depressurization begins and combined with the initial tank conditions to estimate the jet velocity and flow rate described in Section 2.3.

Just before depressurization, the sum of the partial volumes of the liquid mass, M_{Ld}, and vapor mass, M_{Vd}, still equals the tank volume:

$$V_{tank} = M_{Ld} / \rho_{Ld} + M_{Vd} / \rho_{Vd} \quad [4]$$

The depressurization point liquid density, ρ_{Ld}, and vapor density, ρ_{Vd}, correspond to the saturation temperature at the reduced tank pressure. The energy required to create the vapor mass comes from cooling the current liquid and vapor contents in the tank. Assuming the liquid heat capacity, $C_{pL,TIC}$, and vapor heat capacity, $C_{pV,TIC}$, are constant over the temperature range (which they essentially are), the energy balance can be based on the average liquid and vapor masses. The temperature decrease, $\Delta T = T_{air} - T_{tank}$, is written as:

$$\Delta T = M_{Vd} (\Delta H_{v,tank} + \Delta H_{vd}) / [(M_{tank} + M_{Ld}) C_{pL,TIC} + M_{Vd} C_{pV,TIC}] \quad [5]$$

where T_{air} is the ambient temperature, T_{tank} is the tank temperature, $\Delta H_{v,tank}$ is the heat of vaporization at the tank temperature, and ΔH_{vd} is the heat of vaporization at the tank temperature prior to depressurization. Since additional mass vaporizes as the tank depressurizes, the masses of vapor and liquid cannot be determined from just Equations [4] and [5].

The depressurization occurs adiabatically, so enthalpy is conserved, and the energy and mass balances are:

$$M_{Ld} H_{Ld} + M_{Vd} H_{Vd} = M_R H_L + M_{Vc} (H_{Vd} + H_V)/2 + M_{hs} H_V \quad [6]$$

$$M_{Ld} + M_{Vd} = M_R + M_{Vc} + M_{hs} \quad [7]$$

H_{Ld} and H_{Vd} are the enthalpies of liquid and vapor at the depressurization temperature, and H_L and H_V are the enthalpies of liquid and vapor at the boiling temperature. These equations include both the vapor leaving the tank as part of the source cloud, M_{Vc}, and the vapor remaining in the head space in order to represent the closed system of vapor and liquid masses. The temperature of the vapor leaving the tank decreases from the tank temperature at the point of depressurization to the boiling temperature when auto-refrigeration is complete. For constant vapor heat capacity, the average of the vapor enthalpies is used.

The *PV* work terms relevant to Equations [5] and [6] are negligible compared to the enthalpy terms. This set of equations must be solved iteratively. The procedure is:

(1) Select ΔT and determine ρ_{Ld}, ρ_{Vd}, H_{Ld}, and H_{Vd} from saturation tables.

(2) Rearrange Equation [4] to solve for M_{Ld}, substitute it into Equation [5], and solve for the vapor mass before depressurization:

$$M_{Vd} = (M_{tank} + V_{tank}\,\rho_{Ld})C_{pL,TIC} / [(\Delta H_{v,tank} + \Delta H_{vd})/\Delta T + C_{pL,TIC}\,\rho_{Ld}/\rho_{Vd} - C_{pV,TIC}] \quad [8]$$

(3) Solve Equation [4] using M_{Vd} for the liquid mass in the tank before depressurization.

(4) Solve Equation [7] for the vapor mass leaving the tank.

(5) Compute the total enthalpy before depressurization, H_d:

$$H_d = M_{Ld}\,H_{Ld} + M_{Vd}\,H_{Vd} \quad [9]$$

(6) Compute the total enthalpy after auto-refrigeration, H_{tank}:

$$H_{tank} = M_R\,H_L + M_{Vc}\,(H_{Vd} + H_V)/2 + M_{hs}\,H_V \quad [10]$$

(7) If H_d is less than H_{tank} lower the temperature and repeat, and vice versa, until converged.

2.3 Velocity and Flow Rate

Experiments with releases of superheated liquids through nozzles have shown that even well into the superheated range (up to around 20 °C), large droplets (several hundred microns in diameter) form through breakup mechanisms.[5-9] Ammonia droplets larger than 200 microns in diameter have been calculated to be large enough to reach the ground without evaporating from release heights of several meters.[5] Since chlorine has the same boiling temperature, droplet evaporation rates are comparable. At very high superheat (greater than 40 °C) small droplets form. These droplets tend to be on the order of 20–30 microns in diameter.[5, 9] Rainout of large droplets at high superheat has been found to be minimal, suggesting that the fraction of larger droplets is very small. The transition from formation of large droplets with significant rainout to formation of small droplets with minimal rainout occurs around 20 °C to 40 °C superheat. It is assumed that the derivations here are applicable down to 20 °C of superheat, with the realization that total cloud mass decreases due to rainout of larger droplets.

For typical ambient wind conditions, droplets smaller than 10–20 microns do not deposit onto surfaces due to gravitational settling because small turbulence eddies keep them airborne. Droplets of all sizes still deposit due to inertial and diffusion forces. It is likely that the liquid aerosol will coat the ground surface and vegetation under the cloud, but that much of the aerosol will not settle before it evaporates from the energy added by air entrained at the cloud top surface. It is assumed that agglomeration of aerosol to form larger droplets is not significant. Any liquid coating the surface will evaporate quickly once the cloud from which it came is gone.

At storage pressures of 5-11 atm, the experimentally measured velocity of the jet exiting a nozzle, *v*, is approximately 20 m/s.[9] The relevant equation for the liquid flow is the Bernoulli equation which relates jet kinetic energy to tank pressure, P_{tank}, plus liquid head pressure, $P_{head} = \rho_{tank}\,g\,\Delta h$, minus ambient pressure, P_{atm}:

$$P_{tank} + P_{head} - P_{atm} = \rho_{tank}\, v^2/(2\, C_D^2) \quad [11]$$

where g is the gravitational acceleration constant, and Δh is the height between the hole and the vapor-liquid interface. The orifice discharge coefficient, C_D, accounts for frictional losses within the hole and is normally set to 0.6. The tank fluid density, ρ_{tank}, is expected to be that of the liquid at the tank temperature; however, if vapor nucleation occurs prior to the orifice, the effective two-phase density can be used. For the incidents considered here, the tank pressure and liquid density both decrease between the time of hole formation and the time at which the vapor-liquid interface reaches the hole. The tank equilibrium calculations in Section 2.2 predict that these values do not change greatly.

Jet velocity according to the Bernoulli equation is independent of hole area, as long as the discharge coefficient is not altered. The Bernoulli equation assumes that the thickness of the hole is negligible. A chlorine railcar tank is ¾ inch thick and has 4 inches of insulation and a ⅛ inch thick metal jacket; the hole length is therefore 4.875 inches (0.124 m). A hole in a chlorine railcar thus has a significant thickness, so the jet experiences friction losses between the opening inside the tank and the opening to ambient air. The degree to which the hole is jagged or smooth can vary significantly for different breaching scenarios, as can the uniformity of the hole diameter across the three layers in a railcar. For the purposes of the calculations in this work, the hole interior surface is assumed to be smooth with a constant diameter. In this case friction losses for flow through a pipe apply. The friction factor, f , is defined as:

$$f = \Delta P\, d/(2\, \rho_{tank}\, v^2\, L) \quad [12]$$

where d is the hole diameter, L is the hole length, and ΔP represents the loss in pressure along the length of the hole.

Flow through a pipe is considered fully turbulent for Reynolds numbers, $Re = d\, v\, \rho_{tank}/\mu_{TIC}$, greater than 10,000, where μ_{TIC} is the viscosity of the liquid in the tank. The friction factor for smooth pipes is given by the Blasius equation, $f = 0.079\, Re^{-0.25}$, while the friction factor for the roughness associated with commercial pipe is slightly different:[10]

$$f = 0.04\, Re^{-0.16} \quad [13]$$

Equating Equation [12] with Equation [13] and rearranging gives the pressure drop along the length of the hole:

$$\Delta P = 0.08\, L\, \rho_{tank}^{0.84}\, v^{1.84}\, \mu_{TIC}^{0.16}/d^{1.16} \quad [14]$$

This pressure drop is subtracted from the tank pressure in the Bernoulli equation to give the jet velocity adjusted for frictional losses through the length of the hole:

$$v = C_D\, [2\, (P_{tank} + P_{head} - \Delta P - P_{atm})/\, \rho_{tank}]^{0.5} \quad [15]$$

These equations must be solved iteratively. Note that, if the pressure in the tank at the hole equals the chemical saturation pressure, even this small pressure drop leads to flashing before the orifice. In this case, Equations [12] through [15] do not apply; only Equation [11] is used with the appropriate fluid density. What leads to frictional losses in the pipe for liquid flow now determines the fraction of liquid flashing before the orifice.

The flow rate, Q, for the jet becomes a simple function of hole area:

$$Q = \rho_{Tank}\, v\, \pi\, d^2/4 \quad [16]$$

Tank empty time, t_f, is:

$$t_f = M_{TIC}/Q \quad [17]$$

Vapor mass from depressurization and auto-refrigeration has been included in this calculation, as it comprises only a small fraction of the total chemical mass released.

2.4 Chlorine Expansion to Ambient

As the liquid passes through the hole, some liquid vaporizes to equilibrate at ambient pressure. The remaining liquid breaks up into aerosol and droplets due to either mechanical or vapor nucleation forces. The vapor expansion is adiabatic, as no energy is added to the chlorine as it passes through the hole. No work is done on the liquid, either, so enthalpy is conserved. The vapor expansion outside of the hole occurs in all directions, although some fluid acceleration in the jet direction may occur due to backpressure from within the orifice. As long as liquid remains during the adiabatic expansion, the cloud forms at saturation temperature at the ambient pressure (i.e., the boiling temperature). These conditions apply just outside of the hole and prior to the ambient air entrainment addressed in Section 2.5.

The fraction of vapor in the two-phase jet can be determined for an arbitrary starting mass of chemical:[6]

$$M_{TIC} = M_L + M_V \quad [18]$$

$$M_{TIC}\, H_{TIC} = M_L\, H_L + M_V\, H_V \quad [19]$$

H_{TIC} represents the enthalpy at the tank temperature. M_L and M_V represent the resulting liquid and vapor masses following adiabatic expansion. The liquid and vapor enthalpy values are at the boiling temperature as used in Section 2.2. The chemical mass represents a control volume mass passing from inside the tank to outside the tank. Note that this derivation maintains that the fluid velocity does not change. Defining a vapor mass fraction in the jet, $F_J = M_V/M_{TIC}$, Equations [18] and [19] can be combined:

$$F_J = (H_{TIC} - H_L) / (H_V - H_L) \quad [20]$$

Contributions from ρ_V volumetric expansion and the surface tension energy of the small droplets are negligible.

The volume of mass released, V_{TIC}, is the sum of the liquid and vapor partial volumes:

$$V_{TIC} = M_L / \rho_L + M_V / \rho_V \quad [21]$$

The density of the two-phase jet, ρ_J, is:

$$\rho_J = \rho_L\, \rho_V / [(1 - F_J)\, \rho_V + F_J\, \rho_L] \quad [22]$$

2.5 Air Entrainment into the Jet

After expanding to atmospheric pressure, the jet interacts with the ambient air surrounding the hole. The entrainment ratio, $E = V_{air}/V_{TIC}$, is defined as the volume of ambient air, V_{air}, added to the jet over the volume of the chemical vapor and liquid. For this application only air mixing into the jet close to the hole is considered. The best example involves an instantaneous release of the tank contents as a large cloud, where the air within that cloud volume mixes with the chemical instead of being displaced. Subsequent entrainment of air at the cloud or jet edges as it moves downwind is not relevant to the processes addressed in this paper.

Ambient air contains water vapor in addition to the nitrogen, oxygen, and other gases in dry air. The mass fraction of water vapor in ambient air, F_{H2O}, is:

$$F_{H2O} = RH\ P_{s,H2O}\ W_{H2O}/[RH\ P_{s,H2O}\ W_{H2O} + (P_{atm} - RH\ P_{s,H2O})\ W_{air}] \quad [23]$$

where RH is the relative humidity, $P_{s,H2O}$ is the vapor pressure of water, W_{H2O} is the molecular weight of water, and W_{air} is the molecular weight of dry air. The partial densities of dry air, $\rho_{air,dry}$, and water vapor, ρ_{H2O}, are determined using the ideal gas law:

$$\rho_{air,dry} = (P_{atm} - RH\ P_{s,H2O})\ W_{air}/[(1000\ g/kg)\ R\ T_{air}] \quad [24]$$

$$\rho_{H2O} = RH\ P_{s,H2O}\ W_{H2O}/[(1000\ g/kg)\ R\ T_{air}] \quad [25]$$

where R is the ideal constant. The moist air density, ρ_{air}, is the sum of these partial densities. Mixing is assumed to be rapid enough and the chemical droplets small enough that they do not rain out of the cloud before equilibrium is achieved. For expected entrainment ratios, the energy available from the air and water is not sufficient to vaporize all the droplets. Energy from the air and water is used to convert chemical liquid into vapor, so the air and water will cool. For the small chemical droplets present, heat and mass transfer are very rapid, so the droplet temperature is not depressed during this period of evaporation. The mixed cloud reaches temperature equilibrium when all components are at the chemical boiling temperature and ambient pressure. However, since the chemical vapor can no longer be at the equilibrium vapor pressure of 1 atm (101.325 kPa) with entrained air present, vapor-liquid equilibrium no longer exists. The partial pressure of chemical vapor cannot be raised, so the only means to achieve vapor-liquid equilibrium is to lower the equilibrium pressure by cooling the cloud until the chlorine vapor pressure equals the chlorine vapor partial pressure. The energy to cool the cloud comes from evaporating yet more chlorine liquid, using the chemical heat of vaporization to generate the temperature decrease. Since all partial pressures decrease with decreasing temperature, additional chemical vapor is generated in this closed system without exceeding ambient pressure. This process is called homogeneous equilibrium and results in a cloud temperature below the chemical boiling temperature.[11]

The equilibrium processes affecting each cloud component are somewhat different. The entrained dry air cools from ambient temperature to the final cloud temperature without any change of phase. The water vapor mass in air cools from ambient temperature to the final cloud temperature. Almost all of the water mass forms ice crystals. Remaining water vapor simply cools from ambient temperature to the final cloud temperature. The mass fraction of water vapor remaining, F_{wv}, is a function of ice vapor pressure, $P_{s,ice}$, at the final cloud temperature:

$$F_{wv} = P_{s,ice}/RH\ P_{s,H2O} \quad [26]$$

Chemical liquid and vapor in the cloud cools from the boiling temperature to the final cloud temperature. The energy change, ΔU, for each component becomes:

$$\Delta U_{air,dry} = M_{air,dry}\ C_{p,air}\ (T_{air} - T_c) \quad [27]$$

$$\Delta U_{H2O} = F_{wv}\ M_{H2O}\ C_{pV,H2O}\ (T_{air} - T_c) \quad [28]$$

$$\Delta U_{ice} = (1 - F_{wv})\ M_{H2O}\ [\Delta H_{v,H2O} + C_{pL,\ H2O}\ (T_{air} - T_{f,H2O}) + \Delta H_{f,H2O} + C_{pS,H2O}\ (T_{f,H2O} - T_c)] \quad [29]$$

$$\Delta U_L = ((1 - F_J)\ M_{TIC} - M_{VE})\ C_{pL,TIC}\ (T_b - T_c) \quad [30]$$

$$\Delta U_V = (F_J\, M_{TIC} + M_{VE})\, C_{pV,TIC}\, (T_b - T_c) \quad [31]$$

where T_c is the final cloud temperature, T_b is the boiling temperature, $M_{air,dry}$ and M_{H2O} are the entrained dry air and water masses, $C_{p,air}$ and $C_{pV,H2O}$ are the heat capacities of dry air and water vapor, $\Delta H_{v,H2O}$ and $\Delta H_{f,H2O}$ are the heats of vaporization of water and fusion of ice, $C_{pL,\,H2O}$ and $C_{pS,H2O}$ are the heat capacities of water and ice, $T_{f,H2O}$ is the freezing temperature of water, and M_{VE} is the additional mass of chemical vaporized to reach equilibrium.

The entrained dry air mass and water mass can be related to chemical cloud mass using volume as mass divided by density:

$$M_{air,dry} = (1 - F_{H20})\, \rho_{air}\, E\, M_{TIC} / \rho_J \quad [32]$$

$$M_{H2O} = F_{H20}\, \rho_{air}\, E\, M_{TIC} / \rho_J \quad [33]$$

All energy from cooling and water phase change is used to convert chemical liquid to vapor:

$$M_{VE}\, \Delta H_{v,TIC} = \Delta U_{air,dry} + \Delta U_{H2O} + \Delta U_{ice} + \Delta U_L + \Delta U_V \quad [34]$$

where $\Delta H_{v,TIC}$ is the heat of vaporization of the chemical at its boiling temperature. Equations [27] through [33] can be substituted into Equation [34] to put all energy components in terms of cloud mass. The equation can then be solved for a defined mass evaporation ratio, $\alpha = M_{VE} / M_{TIC}$:

$$\alpha = (\{(1 - F_{H20})\, C_{p,air}\, (T_{air} - T_c) + F_{wv}\, F_{H20}\, C_{pV,H2O}\, (T_{air} - T_c) + (1 - F_{wv})\, F_{H20}\, [\Delta H_{v,H2O} + C_{pL,\,H2O}\, (T_{air} - T_{f,H2O}) + \Delta H_{f,H2O} + C_{pS,H2O}\, (T_{f,H2O} - T_c)]\} E\, \rho_{air} / \rho_J + [(1 - F_J) C_{pL,TIC} + F_J\, C_{pV,TIC}](T_b - T_c)) / [\Delta H_{v,TIC} + (C_{pL,TIC} - C_{pV,TIC})(T_b - T_c)] \quad [35]$$

The only unknown terms in Equation [35] are the final cloud temperature and water vapor mass fraction, with the water vapor mass fraction determined at the final cloud temperature using Equation [26].

The chlorine masses can be written as:

$$M_L = (1 - F_J - \alpha)\, M_{TIC} \quad [36]$$

$$M_V = (F_J + \alpha)\, M_{TIC} \quad [37]$$

The maximum entrainment ratio occurs when the energy balance results in all chemical liquid evaporation. According to these equation, this situation occurs when $\alpha = 1 - F_J$. The maximum entrainment ratio is much higher than assumed for the type of incident considered here.

2.6 Cloud Equilibrium

Determining the final cloud temperature requires a separate equation for chemical vapor partial pressure, P_V:

$$P_V = (1000\ g/kg)\, M_V\, R\, T_c / W_{TIC}\, V_c \quad [38]$$

where W_{TIC} is the toxic industrial chemical molecular weight, and V_c is the cloud volume. At their boiling temperatures, the chlorine vapor pressure from the ideal gas equation is two percent less than that from

the saturation table[12] and the ammonia vapor pressure is 5 percent less than from the saturation table.[10] Therefore, for cloud temperatures below the chemical boiling temperature, then, ideal gas behavior is assumed to be valid for the vapor components of the cloud. At the final cloud temperature, the chlorine partial pressure equals the chlorine saturation pressure, $P_V = P_{s,TIC}$.

The cloud component volumes, V, are determined using mass divided by pure component density using the mass relations presented in Section 2.5, with the densities of chemical vapor, dry air, and water vapor are computed using the ideal gas equation:

$$V_L = (1 - F_J - \alpha)\, M_{TIC} / \rho_{cL} \quad [39]$$

$$V_V = (1000\ g/kg)\, R\, T_c\, (F_J + \alpha)\, M_{TIC} / P_{atm}\, W_{TIC} \quad [40]$$

$$V_{air} = (1000\ g/kg)\, R\, T_c\, (1 - F_{H20})\, \rho_{air}\, E\, M_{TIC} / \rho_J\, P_{atm}\, W_{air} \quad [41]$$

$$V_{H2O} = (1000\ g/kg)\, R\, T_c\, F_{H20}\, F_{wv}\, \rho_{air}\, E\, M_{TIC} / \rho_J\, P_{atm}\, W_{H2O} \quad [42]$$

$$V_{ice} = F_{H20}\, (1 - F_{wv})\, \rho_{air}\, E\, M_{TIC} / \rho_J\, \rho_{ice} \quad [43]$$

where ρ_{cL} is the density of liquid chlorine at the final cloud temperature, and ρ_{ice} is the density of ice. Cloud volume is given by the sum of Equations [39] through [43]. Substituting this sum plus the vapor mass represented by Equation [37] into Equation [38] gives the chemical vapor partial pressure in terms of final cloud temperature and mass evaporation ratio:

$$P_V = (1000\, R\, T_c / W_{TIC})\, (F_J + \alpha) / ((1 - F_J - \alpha) / \rho_{cL} + 1000\, R\, T_c\, (F_J + \alpha) / P_{atm}\, W_{TIC} + (E\, \rho_{air} / \rho_J)\{(1000\, R\, T_c / P_{atm})[(1 - F_{H20}) / W_{air} + F_{H20}\, F_{wv} / W_{H2O}] + F_{H20}\, (1 - F_{wv}) / \rho_{ice}\}) \quad [44]$$

As with the tank equilibrium calculations in Section 2.2, there is no direct solution for the final cloud temperature. The iterative procedure is:

(1) Assume a final cloud temperature below the chlorine boiling point and determine ρ_{cL}, $P_{s,ice}$, and $P_{s,TIC}$ from saturation tables.

(2) Calculate the fraction of water vapor remaining using Equation [26].

(3) Calculate the mass evaporation ratio using Equation [35].

(4) Calculate the chemical vapor partial pressure using Equation [44].

(5) If the saturation pressure exceeds the chemical vapor partial pressure, decrease the final cloud temperature, and vice versa, and repeat until converged.

Cloud mass, M_c, equals:

$$M_c = M_{TIC}\, (1 + E\, \rho_{air} / \rho_J) \quad [45]$$

Cloud density, ρ_c, is given by the cloud mass divided by the cloud volume:

$$\rho_c = (1 + E\, \rho_{air} / \rho_J) / ((1 - F_J - \alpha) / \rho_{cL} + 1000\, R\, T_c\, (F_J + \alpha) / P_{atm}\, W_{TIC} + (E\, \rho_{air} / \rho_J)\{(1000\, R\, T_c / P_{atm})[(1 - F_{H20}) / W_{air} + F_{H20}\, F_{wv} / W_{H2O}] + F_{H20}\, (1 - F_{wv}) / \rho_{ice}\}) \quad [46]$$

The corresponding cloud concentration, C, is given by the total chemical mass divided by the cloud volume:

$$C = 1/((1 - F_J - \alpha)/\rho_{cL} + 1000\ R\ T_c\ (F_J + \alpha)/P_{atm}\ W_{TIC} + (E\ \rho_{air}/\rho_J)\{(1000\ R\ T_c/P_{atm})[(1 - F_{H20})/W_{air} + F_{H20}\ F_{wv}/W_{H2O}] + F_{H20}\ (1 - F_{wv})/\rho_{ice}\}) \quad [47]$$

2.7 Mist Pool Theory

Modern dense gas hazard assessment models use the calculations in the preceding sections, with some variation. Results applying these equations for a recent chlorine railcar incident at Macdona, Texas[13] for a corresponding Transportation Security Administration study are comparable to those generated using two proprietary dense gas models.[1] The above results are included to support the mist pool theory presented in this section. Given release of a toxic industrial chemical through a hole or rupture as a two-phase jet, all existing dense gas models assume that the two phase jet continues to exchanges mass, momentum, and energy with the surrounding ambient air. This continued air entrainment quickly dilutes the cloud and its density, so the cloud mass is carried downwind at a rate determined by the wind velocity and loss of initial momentum. If the slow vapor flux from boiling liquid remaining in the tank or evaporating from pooled liquid rained out from the jet is ignored, the models predict that as soon as the tank empty process is complete, the chemical quickly leaves the incident area.

These model predictions are in stark contrast to some observations where chlorine vapor has remained in terrain depressions, been blocked by tree lines, or collected in valleys for extended periods of time.[13-17] These observations suggest that there are conditions for which the passing ambient air cannot effectively remove the chemical as it exits the hole. The result is an accumulation of chemical vapor and aerosol that persists at the incident location for a measurable period of time beyond the tank empty time. This cloud of highly dense chemical vapor and aerosol is defined as a mist pool. This paper derives a criterion that can be used to estimate when a mist pool will form and provides the equations characterizing the behavior of a mist pool once it has formed. The calculations are then applied to the example chlorine and ammonia incidents.

A mist pool is proposed to form when the rate of toxic industrial chemical passing through the hole exceeds the capacity of the air to remove it from the incident location. The chemical vapor and aerosol that is not taken up by passing air collects at the incident site, continuing to add to the accumulated cloud mass until the tank empty time is reached. The high cloud density leads to the slumping behavior that dense gas models already treat for instantaneous releases. The cloud radius expands over flat and unobstructed terrain, with considerable turbulence within. Observations from field trials suggest the visible cloud height stabilizes at approximately 1 m.[18-25] The final cloud form becomes a flat cylinder of large diameter. Air is entrained by the combined events of interaction of the jet with passing air and turbulent entrainment at the cloud edges. Since the entrainment ratio with passing air is reduced, the entrainment at the cloud edges is assumed to balance that reduction to lead to an entrainment ratio comparable to the jet calculations in Section 2.6, which is assumed to Equation [5]. The cloud, which contains the combined mass of chemical vapor and aerosol, air, water vapor, and ice, can be represented by a 1 m thick disk with the components uniformly distributed throughout:

$$M_c = \pi \rho_c D_c^2 H_c/4 \quad [48]$$

where D_c is the cloud diameter, and H_c is the cloud height or thickness. If the average mass flow rate through the hole is considered and it is assumed that the cloud height is constant, the cloud diameter can

be represented as a function of time:

$$D_c = [4\ Q\ (1 + E\ \rho_{air}/\ \rho_J)/\pi\ \rho_c\ H_c]^{0.5}\ t^{0.5} \quad [49]$$

where t represents time from hole formation. Although the cloud diameter increases with $t^{0.5}$, the cloud top area increases linearly with time. The average cloud top area during cloud formation is then just half the final cloud top area.

If a mist pool forms according to the criterion proposed below in Section 2.8, the cloud is not moved by the wind. Rather, it remains stationary and provides an area vapor flux to the passing air until it is depleted. The concept of a stationary area vapor source is not new. The HGSYSTEM[26] and DEGADIS[27, 28] models address the situation where the rate of vapor formation from an evaporating liquid pool exceeds the capability of the passing air to remove it. An expanding secondary source blanket is then formed above the liquid pool and is treated as a stationary vapor source, with vapor exchange to the passing air at the cloud top. This situation persists until vapor generation conditions change. The area vapor source approach has not yet been applied to the vapor, aerosol, and entrained air mix from a two-phase jet. The mist pool theory in this paper extends the secondary source blanket approach used by HGSYSTEM and DEGADIS.

2.8 Mist Pool Formation Criterion

The HGSYSTEM and DEGADIS models both compute a maximum entrainment or take-up rate based on the area of the top surface of the secondary source blanket. As long as the mass flux from the evaporating pool exceeds the maximum entrainment rate, the resulting cloud remains centered at the release location and increases in mass equal to the difference between the rates. Once no additional mass is being generated or the mass rate becomes less than the maximum, the models decrement the cloud mass by the maximum entrainment rate until no vapor remains. The mist pool process proposed here applies the same maximum entrainment rate to the jet from railcar incidents. If the mass flow rate through the hole does not exceed the maximum entrainment rate, no stationary cloud forms. In this case, the existing modeling capability (e.g., in HGSYSTEM, DEGADIS, and other modern dense gas models) is considered appropriate.

Entrainment rates are computed by dense gas models to estimate the rate of mass transfer across the effective surface boundary between ambient air and the cloud or jet. The typical use is to determine the rate of entrainment of ambient air into the cloud or jet mass; however, the entrainment rates are not directional, so they can just as readily be used to estimate the entrainment of chemical from the jet into ambient air. The HGSYSTEM and DEGADIS models contain similar entrainment rate equations for both directions, the use of which becomes situation dependent. The vertical entrainment velocity is a function of the Richardson number, Ri_*:

$$Ri_* = g\ (\rho_c - \rho_{air})\ H_c/\ \rho_{air}\ u_*^2 \quad [50]$$

where u_* is the friction velocity for the ambient wind conditions. By itself, the Richardson number provides an estimate of the relative resistance of the cloud mass to the passing air. Vertical entrainment velocity, w_*, for the secondary source blanket in DEGADIS[27, 28] is given as:

$$w_* = 0.735\ u_*\ (1 + a)/(0.88 + 0.046\ Ri_*^{1.04}) \quad [51]$$

In this equation, a equals the exponent for the vertical wind profile power law equation. Pulling together all contributions to the vertical entrainment velocity from HGSYSTEM simplifies to:[26]

$$W_* = 2.87\ u_*/Ri_* \quad [52]$$

for $Ri_* > 12$. An alternate relation is used for lower Richardson numbers:

$$w_* = 0.70\ u_*/(1 + 0.8\ Ri_*)^{0.5} \quad [53]$$

A third equation for vertical entrainment velocity is given by Briggs[29]:

$$w_* = 0.65\ u_*/(1 + 0.2\ Ri_*) \quad [54]$$

The vertical entrainment velocity equations were derived from data on all-vapor sources with Richardson numbers up to about 20;[29] given the lack of experimental data and equations for two-phase entrainment velocities, the relations described above are used.

The vertical entrainment predictions were compared for three ambient wind conditions, all for a grassy surface (5 cm roughness length) on open terrain: unstable conditions with a 2 m/s wind speed at 2 m above the ground surface, neutral conditions with a 5 m/s wind speed, and stable conditions with a 2 m/s wind speed. Three conditions for the chlorine and ammonia incidents were considered: cloud formation (Ri_* from 24 to 2087), no remaining aerosol (Ri_* from 6 to 689), and a Richardson number of zero. The cloud density after all aerosol has evaporated, ρ_{cf}, is obtained by subtracting the liquid aerosol mass and partial volume from Equation 46:

$$\rho_{cf} = (F_J + \alpha + E\ \rho_{air}/\rho_J)/(1000\ R\ T_c\ (F_J + \alpha)/P_{atm}\ W_{TIC} + (E\ \rho_{air}/\rho_J)\{(1000\ R\ T_c/P_{atm})[(1 - F_{H2O})/W_{air} + F_{H2O}\ F_{wv}/W_{H2O}] + F_{H2O}\ (1 - F_{wv})/\rho_{ice}\}) \quad [55]$$

The corresponding cloud concentration, C_f, is needed to estimate mass flux:

$$C_f = (F_J + \alpha)/(1000\ R\ T_c\ (F_J + \alpha)/P_{atm}\ W_{TIC} + (E\ \rho_{air}/\rho_J)\{(1000\ R\ T_c/P_{atm})[(1 - F_{H2O})/W_{air} + F_{H2O}\ F_{wv}/W_{H2O}] + F_{H2O}\ (1 - F_{wv})/\rho_{ice}\}) \quad [56]$$

The comparison of the velocities shows a typical range of about a factor of 5 across the three model approaches. The HGSYSTEM and Briggs equations produce very similar values for all conditions, while the DEGADIS equations always result in the highest velocity. The HGSYSTEM equations have been selected for mist pool vapor flux computations.

The maximum mass entrainment rate, Q_v, at the cloud top equals $Q_v = A\ f_v$, where f_v is the vapor mass flux and A is the cloud top area. The area equals half the final cloud top area. Vapor mass flux is given by $f_v = C\ w_*$. The maximum entrainment rate equation for $Ri_* > 12$ becomes:

$$Q_v = 2.87\ C\ u_*\ \pi\ D_c^2/8\ Ri_* \quad [57]$$

The proposed criterion for mist pool formation is that the ratio of the maximum entrainment rate over jet flow rate, Q_v/Q, be less than one.

Additional consideration must be made for the fact that the vertical entrainment velocity equations were derived from data taken over homogeneous, flat terrain and do not account for the orientation of the jet. A jet orientation resists being taken up by the passing air when it is pointing into the wind, or downward. When the initial cloud behavior is dominated by gravitational slumping, terrain slope and depressions affect cloud stability. Any mass settling into terrain depressions resists being removed by the air. Finally, obstructions such as buildings and tree stands provide a barrier to cloud movement. If buildings or trees obstruct the initial cloud movement, it resists being moved by the wind. The effects of the jet aiming upwind or downward, terrain depressions, and building and tree obstructions are roughly approximated by decreasing the entrainment velocity (and thus the entrainment rate) by the factor of 5 found to represent

the spread of entrainment velocities under normal open terrain conditions. Enhanced entrainment from the jet aiming with the wind is likewise accounted for using a factor of 5 increase. The first conditions are referred to here as sheltered and the latter as enhanced. Equation [57] is rewritten as the mist pool formation criterion with the entrainment factor, *B*:

$$Q_v/Q = 2.87\ B\ C\ \rho_{air}\ u_*^3\ \pi D_c^2/[8\ Q\ g\ (\rho_c - \rho_{air})\ H_c] < 1 \qquad [58]$$

where B = 5 for enhanced entrainment, 1 for normal entrainment, and 0.2 for sheltered entrainment. Note that the ratio increases strongly with increases in friction velocity and final cloud diameter and decreases linearly with increases in jet mass flow rate and cloud height. The cloud concentration and density are related; the effect is that the ratio changes slowly with air entrainment ratio and jet density. Ratios close to unity signify that if a mist pool forms, it will only last a short while beyond the tank empty time. If a mist pool does not form, the cloud mass will not be easily moved by the passing wind, and parts of it will be retained within terrain depressions and blocked by obstructions. A combination of bulk cloud movement at reduced speed with a significant vapor flux into passing air is likely.

2.9 Mist Pool Vapor Flux

The mist pool process proposed for massive releases of toxic industrial chemical follows three stages. The criterion in Section 2.8 determines if a mist pool is expected to form under the release conditions. If a mist pool does not form, the normal dense gas modeling of the jet applies.

2.9.1 Tank Emptying

During the first stage, the cloud expands as a disk of constant height with a diameter given by Equation [49]. This stage continues until the tank empty time is reached. For conditions meeting the mist pool criterion, this time is several minutes or less. Chemical vapor is entrained at the cloud top during this stage. It is assumed that all vapor lost is replaced by evaporated aerosol, so the cloud density, chlorine concentration, and Richardson number all decrease somewhat. The dynamic conditions keep the cloud well mixed throughout.

The average entrainment rate during stage 1, Q_{v1}, is given by Equation [57]. In order to account for the mass lost during this stage the fraction of aerosol mass remaining, $1 - F_J - \alpha - Q_{v1}/Q$, is determined. The cloud density, ρ_{c1}, and concentration, C_1, are recalculated for this additional aerosol mass lost:

$$\rho_{c1} = (1 + E\ \rho_{air}/\rho_J - Q_{v1}/Q)/((1 - F_J - \alpha - Q_{v1}/Q)/\rho_{cL} + 1000\ R\ T_c\ (F_J + \alpha)/P_{atm}\ W_{TIC} + (E\ \rho_{air}/\rho_J)\{(1000\ R\ T_c/P_{atm})[(1 - F_{H20})/W_{air} + F_{H20}\ F_{wv}/W_{H2O}] + F_{H20}\ (1 - F_{wv})/\rho_{ice}\}) \qquad [59]$$

$$C_1 = (1 - Q_{v1}/Q)/((1 - F_J - \alpha - Q_{v1}/Q)/\rho_{cL} + 1000\ R\ T_c\ (F_J + \alpha)/P_{atm}\ W_{TIC} + (E\ \rho_{air}/\rho_J)\{(1000\ R\ T_c/P_{atm})[(1 - F_{H20})/W_{air} + F_{H20}\ F_{wv}/W_{H2O}] + F_{H20}\ (1 - F_{wv})/\rho_{ice}\}) \qquad [60]$$

The Richardson number and average entrainment rate are then recalculated using Equations [50] and [57], respectively. The aerosol mass remaining at the end of stage 1 is then calculated as $M_{L1} = (1 - F_J - \alpha - Q_{v1}/Q)\ M_{TIC}$. If the aerosol mass remaining becomes less than zero for either this equation or the estimate before recalculation, the aerosol evaporates as the tank empties, and the average entrainment rate is reset to $Q_{v1} = (1 - F_J - \alpha)\ Q$. Chemical mass at the end of stage 1 equals $M_1 = M_{TIC} - Q_{v1}\ t_f$.

2.9.2 Aerosol Evaporation

During the second stage, the cloud maintains a constant diameter and generates vapor from the cloud top surface. The vapor flux is replaced by evaporating aerosol. If the aerosol evaporates as the tank empties, this stage is skipped. Any air mass lost with the vapor at the top surface is replaced with an equivalent amount of moist air. The air substitution plus heat flux from the ground surface provide the energy for evaporating the aerosol, and all components are assumed to be well mixed at all times. This assumption should be valid for several minutes beyond the tank empty time, after which the internal cloud turbulence subsides, and aerosol begins to deposit onto the ground surface. Mass deposited as a film on the ground surface below the cloud, though, and then evaporates as part of the all-vapor cloud in the next stage. The vapor flux is assumed constant during this step. As long as aerosol remains, the cloud temperature does not change. Cloud volume decreases slightly with time due to loss of the aerosol, but this insignificant change is ignored. The cloud density, chlorine concentration, and Richardson number decrease steadily as aerosol evaporates.

The entrainment rate at the end of stage 1 equals twice the recalculated value from Equation [57]. The entrainment rate at the end of stage 2 is then calculated as:

$$Q_{vf} = 2.87\ B\ C_f\ u_*\ \pi\ D_c^2/4\ Ri_{*f} \quad [61]$$

where Q_{vf} is the entrainment rate when no aerosol remains and Ri_{*f} is computed using the cloud density after all aerosol has evaporated. The entrainment rate during stage 2, Q_{v2}, is computed as the average of Q_{vf} and that at the end stage 1. The duration of stage 2, t_2, equals $t_2 = M_{L1}/Q_{v2}$, and the chemical mass remaining at the end of stage 2 becomes $M_2 = (F_J + \alpha)\ M_{TIC}$.

2.9.3 Vapor Depletion

The third stage begins when all aerosol mass has evaporated, but it cannot begin before the tank empty time. The vapor mass is assumed to be stripped from the cloud top with no air entrainment into the cloud. The result is a vapor cloud of constant composition that is linearly decreasing in thickness. Cloud density and concentration remain constant, but the Richardson number decreases with the cloud thickness. The starting vapor mass for stage 3 always begins with Equation [68]. During stage 3, the Richardson number crosses a value of 12, so two entrainment equations are needed. The entrainment rate when the Richardson number equals 12, Q_{v3a}, is:

$$Q_{v3a} = 2.87\ B\ C_f\ u_*\ \pi\ D_c^2/(4)(12) \quad [62]$$

The fraction of the cloud height, f_c, when the Richardson number equals 12 is determined next:

$$f_c = \rho_{air}\ u_*^2\ (12)/g(\rho_{cf} - \rho_{air})\ H_c \quad [63]$$

The duration of the first part of stage 3 before the Richardson number reaches 12 is $t_{3a} = 2\ (1 - f_c)\ M_2/(Q_{vf} + Q_{v3a})$. The rate when the last vapor mass is stripped off, Q_{v3b}, is determined for a Richardson number of 0:

$$Q_{v3b} = 0.70\ B\ C\ u_*\ \pi\ D_c^2/4 \quad [64]$$

The duration of the second part following the Richardson number reaching 12 is $t_{3b} = 2\ f_c\ M_2/(Q_{v3a} + Q_{v3b})$.

2.9.4 Combined Vapor Flux

The total mist pool duration, t_{ent}, which includes the tank empty time, equals the sum of four times:

$$t_{ent} = t_f + t_2 + t_{3a} + t_{3b} \quad [65]$$

The average entrainment rate equals $Q_{ent} = M_{TIC} / t_{ent}$. Regardless of the how long the mist pool lasts beyond the tank empty time, the source geometry changes dramatically from a narrow two-phase jet to a large diameter, flat cloud. Note that the entrainment rate increases greatly as the mist pool progresses from cloud formation to all vapor. Based on the very high mass entrainment rates calculated when only vapor remains, the friction velocity will have to be very low in order for a secondary vapor blanket to form. The air will have to be stable and still. With addition of the mist pool aerosol, resistance to entrainment at the cloud top is greatly increased, so a mist pool can form under normal wind conditions for a high jet flow rate.

3.0 RESULTS AND DISCUSSION

Two example incidents are used to demonstrate the mist pool concept; both involve a standard 90-ton railcar. The railcar volume is filled with chlorine and then anhydrous ammonia. It is assumed that the ambient temperature and tank temperature are 20 °C (293.15 K). A full chlorine railcar normally has a small vapor head space or ullage of about 10 percent of the tank volume. To simplify calculations, it is assumed that there is no vapor head space at the time of hole formation. The hole is assumed to be positioned about 1/3 of the way up from the tank bottom to the top, so only liquid is present on the inside at the hole during the release. The final recovered chlorine liquid mass is 20 tons; the recovered ammonia mass is the equivalent volume. Initial chlorine mass is 81,596 kg, and recovered chlorine liquid mass is 18,132 kg. The initial mass of ammonia is determined by relative liquid densities at 20 °C. Physical properties for chlorine and ammonia are provided in Table 1. The initial ammonia mass is 35,328 kg. The liquid densities at the final tank temperature are used to determine the recovered mass of ammonia to be 7931 kg. Tank volume (Equation [1]) is 57.93 m^3. Head space vapor mass (Equation [2]) is 171 kg of chlorine vapor and 42 kg of ammonia vapor. The chlorine incident releases 63,292 kg, and the ammonia incident releases 27,355 kg.

Table 1. Physical Properties of Ammonia and Chlorine

PHYSICAL PROPERTY	VARIABLE	CHLORINE[10, 12, 30]	AMMONIA[10]
boiling temperature (C/K)	T_b	-34.0/239.15	-33.4/239.75
molecular weight (g/mol)	W_{TIC}	70.91	17.03
liquid density at 20 °C (kg/m^3)	$\rho_{L,tank}$	1408.6	609.9
liquid density at T_b (kg/m^3)	ρ_L	1557.9	681.4
vapor density at T_b (kg/m^3)	ρ_V	3.6985	0.9075
heat of vaporization at 20 °C (kJ/kg)	$\Delta H_{v,tank}$	255.13	1188.26
liquid heat capacity (kJ/kg-K)	$C_{pL,TIC}$	0.926	4.65
vapor heat capacity (kJ/kg-K)	$C_{pV,TIC}$	0.50	2.07
liquid enthalpy at T_b (kJ/kg)	H_L	237.64	29.4
vapor enthalpy at T_b (kJ/kg)	H_V	525.72	1401
liquid enthalpy at 20 °C (kJ/kg)	H_{TIC}	288.81	275.19
liquid viscosity (cP)	μ_{TIC}	*	0.12

* no data

3.1 Jet Characterization

The tank emptying equilibrium results (Section 2.2) for the chlorine incident converge at a tank temperature before depressurization of 289.0 K (15.9 °C), or a decrease in temperature of 4.1 °C. The degree of superheat decreases from 54 °C to 50 °C, so it remains very high. The pressure in the tank decreases from 677.9 kPa (6.69 atm) to 606.9 kPa (5.99 atm), and the vapor density decreases from 21.63 kg/m^3 to 19.49 kg/m^3. The liquid density increases slightly from 1408.6 kg/m^3 to 1420.8 kg/m^3. The results for the ammonia incident converge at a tank temperature before depressurization of 290.4 K (17.3 °C), or a decrease in temperature of 2.8 °C. The degree of superheat decreases from 53 °C to 50 °C. The pressure in the tank decreases from 861.3 kPa (8.50 atm) to 792.4 kPa (7.82 atm), and the vapor density decreases from 6.72 kg/m^3 to 6.20 kg/m^3. The liquid density increases slightly from 609.9 kg/m^3 to 613.9 kg/m^3.

A single round hole of 0.10 m diameter (4 inches) is considered for a release from a railcar. The pressure drop through the hole (Equation [14]) is 5.5 kPa (0.054 atm) for the chlorine incident and 7.7 kPa (0.076 atm) for the ammonia incident. The average chlorine jet velocity (Equation [15]) is 18.9 m/s, and the average ammonia jet velocity becomes 34.8 m/s. The final chlorine Reynolds number of 1.49E5 and ammonia Reynolds number of 1.05E5 are both still well into the turbulent flow regime. Both jet velocities are comparable to the value of 20 m/s cited in Section 2.3. Average chlorine flow rate (Equation [16]) is 166 kg/s, and the tank empty time (Equation [17]) is 382 s (6.4 min). The average ammonia flow rate is 121 kg/s, and the tank empty time is 226 s (3.8 min). For the position of the hole in the railcar considered here, the initial liquid head pressure is about 11 to 25 kPa (0.11 to 0.25 atm), so the pressure at the orifice does not reach saturation until the vapor-liquid interface approaches the top of the hole.

The chlorine incident involves expulsion of 59,290 kg of liquid before depressurization and 4002 kg of vapor during depressurization and auto-refrigeration. The ammonia incident involves expulsion of 25,628 kg of liquid before depressurization and 1727 kg of vapor during depressurization and auto-refrigeration. Therefore, 94% of the total chemical mass in each cloud is released prior to depressurization.
For the adiabatic expansion of the jet exiting the hole discussed in Section 2.4, both the chlorine and ammonia jets are 18% vapor and 82% liquid. The density of the chlorine jet (Equation [22]) is 20.8 kg/m^3, and the density of the ammonia jet is 5.1 kg/m^3. The adiabatic expansion leads to an increase in volume of 68 times that of the chlorine liquid inside the tank and 121 times that of the ammonia liquid inside the tank.

For the air entrainment addressed by Section 2.5, physical property values and constants needed for equations dealing with water and air are included in Table 2. Relative humidity is assumed to be 0.50. The resulting water mass fraction (Equation [23]) is 0.0072. At 20 °C and 50% relative humidity, the partial density of dry air (Equation [24]) equals 1.1900 kg/m^3 and the partial density of water vapor (Equation [25]) equals 0.0086 kg/m^3. The moist air density then equals 1.1986 kg/m^3.

The final cloud properties described in Section 2.6 have been determined for an entrainment ratio of 5. The final chlorine cloud temperature is -57 °C, and the saturation pressure is 33.0 kPa (0.325 atm). The fraction of water vapor remaining is 0.0091. 16% of the total chemical cloud mass evaporates in addition to the initial 18% from adiabatic expansion of the jet. The final ammonia cloud temperature is -54 °C, and the saturation pressure is 32.0 kPa (0.316 atm). The fraction of water vapor remaining is 0.0114, and 14% of the cloud mass evaporates in addition to the initial 18%. Achieving both temperature and vapor-liquid equilibrium following initial air entrainment results in both clouds cooling by more than 20 °C below the chemical boiling temperatures. The chlorine incident cloud density (Equation [46]) is 4.9 kg/m^3, or 4.1 times that of ambient air. The ammonia incident cloud density is 2.0 kg/m^3, or 1.7 times that of ambient air. The chlorine concentration (Equation [47]) is 3.8 kg/m^3, and the ammonia cloud concentration is 0.9 kg/m^3. The chlorine cloud density after all aerosol has evaporated (Equation [55]) is 2.4 kg/m^3, and the

corresponding ammonia cloud density is 1.4 kg/m^3. The chlorine and ammonia cloud concentrations after aerosol evaporation (Equation [56]) are 1.3 kg/m^3, and 0.3 kg/m^3, respectively.

Table 2. Other Physical Properties and Contents

PHYSICAL PROPERTY/CONSTANT	VARIABLE	VALUE[10, 31]
water vapor pressure at 20 C (kPa)	$P_{s,H2O}$	2.3
ice vapor pressure at -10 C (kPa)	$P_{s,ice}$	0.27
molecular weight of water (g/mol)	W_{H2O}	18.016
molecular weight of dry air (g/mol)	W_{air}	28.96
water freezing temperature (C/K)	$T_{f,H2O}$	0/273.15
ideal gas constant (m^3-kPa/mol-K)	R	0.008314
gravitational acceleration constant (m/s^2)	g	9.81
Pi	p	3.14159
heat capacity of air (kJ/kg-K)	$C_{p,air}$	1.05
heat capacity of ice (kJ/kg-K)	$C_{pS,H2O}$	1.97
heat capacity of water (kJ/kg-K)	$C_{pL,H2O}$	4.20
heat capacity of water vapor (kJ/kg-K)	$C_{pV,H2O}$	1.88
water heat of fusion (kJ/kg)	$DH_{f,H2O}$	333.7
water heat of vaporization (kJ/kg)	$DH_{v,H2O}$	2261
density of ice (kg/m^3)	r_{ice}	915

3.2 Mist Pool Behavior

For a 1 m cloud height, the chlorine incident mist pool cloud diameter as a function of time (Equation [49]) becomes $D_c = 7.41\ t^{0.5}$, with a final diameter of 145 m. The ammonia cloud diameter as a function of time is $D_c = 12.82\ t^{0.5}$, with a final diameter of 193 m. The mist pool formation criterion derived in Section 2.8 has been applied to the chlorine and ammonia clouds. The entrainment ratio (Equation [58]) for the chlorine incident under neutral conditions (friction velocity of 0.54 m/s) and sheltered entrainment is 0.56, and the ratio for the ammonia incident is 1.48, so a mist pool is expected to form for the chlorine release but not for the ammonia release. The ratios for both incidents are within a factor of two, so relatively small changes in the release conditions can switch the expected behavior.

Since the ammonia incident does not meet the mist pool formation criterion, the vapor flux calculations in Section 2.9 can only be done for the chlorine incident. For the tank emptying stage defined in Section 2.9.1, the initial chlorine entrainment rate is 93 kg/s. The fraction of aerosol remaining becomes 0.10. The cloud density and concentration are recalculated to be 2.8 kg/m^3 and 1.7 kg/m^3, respectively. The Richardson number decreases from 105 to 34, and the average entrainment rate is recalculated to be 96 kg/s. The fraction of aerosol remaining is updated to be 0.08, and the aerosol mass remaining in the cloud at the end of stage 1 is 4965 kg. Chlorine mass in the cloud is 26,472 kg. The average entrainment rate for the aerosol evaporation stage (Section 2.9.2) is 194 kg/s, with a duration of 26 s. The chemical mass remaining is 21,508 kg. The entrainment rate for the first part of the vapor depletion stage (Section 2.9.3) is 376 kg/s with a duration of 37 s. The fraction of the cloud height when the Richardson number reaches 12 is 0.35, so 65% of the vapor mass is stripped off during the first part of that stage. The entrainment rate for the second part of the vapor depletion stage is 1092 kg/s with a duration of 7 s. The total mist pool duration for the chlorine incident is 452 s (7.5 min), with an average entrainment rate of 140 kg/s. Since the tank empty time is 382 s, the mist pool adds only 70 s to the cloud duration at the release location, but other release and atmospheric conditions will result in a mist pool that remains for many minutes after the tank empty time is reached.

4.0 CONCLUSIONS

The mist pool theory predicts that, given appropriate release conditions, the cloud formed from a very large release of superheated liquid over a short release duration does not move with the wind. Rather, the vapor and liquid aerosol collect at the release location as a low, two-phase cloud and remain in place on flat terrain. Vapor is entrained into the passing air through the cloud top surface. The cloud mass is progressively depleted until gone. The overall effect of formation of a mist pool is that the source becomes a large area vapor flux, which lasts significantly longer than the two-phase jet occurring while the tank empties. Modern dense gas models do not include methodology to simulate the processes associated with mist pool formation and, as a result, over-predict concentration versus downwind distance for releases where a mist pool forms. A source module is needed that couples the tank emptying and jet formation processes with the mist pool entrainment calculations. The module would then provide an area flux versus time profile as input to the transport and diffusion module. This paper provides a criterion to predict whether a mist pool is expected to form based on release and atmospheric conditions. The initial methodology requires the user to assume the air entrainment ratio and cloud height, as minimal supporting data exists to provide reliable estimates. Rainout of droplets and reaction/removal mechanisms leading to greater reduction of the cloud density have been ignored in this analysis.

It is important to further consider the mist pool concept because of its dramatic effect on estimation of the toxic effects hazard area. Existing models predict that the size of the hazard area continues to increase with release mass, supporting commonly accepted observations about the most effective atmospheric conditions. Conversely, the mist pool concept suggests that, for very large releases, the toxic effects hazard area is reduced in size due to the extended duration release of contaminant at lower concentrations. The mass resulting in the maximum toxic effects area then becomes the mass just less than that which results in formation of a mist pool. The “most dangerous” atmospheric conditions of lower wind speed and more stable conditions favor mist pool formation. As a result of the findings presented here, the atmospheric conditions resulting in the maximum toxic effects area are concluded to be shifted toward conditions of higher wind speed and turbulence.

5.0 REFERENCES

1. Hanna, Steven R., et al. Comparison of Six Widely Used Dense Gas Dispersion Models for Three Actual Chlorine Railcar Accidents, Wiley Interscience, DOI 10.1002/prs. 10257, 2008.
2. Buckley, R. L.; Hunter, C. H.; Addis, R. P.; Parker, M. J., Modeling dispersion from toxic gas released after a train collision in Graniteville, SC. *J Air Waste Manag Assoc* **2007,** 57, (3), 268-78.
3. Kovalets, I. V.; Maderich, V. S., Numerical simulation of interaction of the heavy gas cloud with the atmospheric surface layer. *Environ. Fluid Mech. FIELD Full Journal Title:Environmental Fluid Mechanics* **2006,** 6, (4), 313-340.
4. Woodward, J. L.; Papadourakis, A., Reassessment and reevaluation of rainout and drop size correlation for an aerosol jet. *J. Hazard. Mater. FIELD Full Journal Title:Journal of Hazardous Materials* **1995,** 44, (2 + 3), 209-30.
5. Paris, A.; Spicer, T.; Havens, J., Modeling the Initial Conditions of Two-Phase Jet Flow through an Orifice after Depressurization, University of Arkansas, Fayetteville, AR. **2006**.
6. Witlox, H.; Harper, M.; Bowen, P.; Cleary, V., Flashing liquid jets and two-phase droplet dispersion II. Comparison and validation of droplet size and rainout formulations. *J Hazard Mater* **2007,** 142, (3), 797-809.
7. Witlox, H. W. M.; Holt, A., A unified model for jet, heavy, and passive dispersion including droplet rainout and re-evaporation. *Int. Conf. Workshop Model. Consequences Accid. Releases Hazard. Mater. FIELD Full Journal Title:International Conference and Workshop on Modeling the Consequences of Accidental Releases of Hazardous Materials, San Francisco, CA, United States, Sept. 28-Oct. 1, 1999* **1999**, 315-344.
8. Kukkonen, J.; Vesala, T.; Kulmala, M., The evaporation of airborne droplets in a turbulent two-phase jet. *J. Aerosol Sci. FIELD Full Journal Title:Journal of Aerosol Science* **1988,** 19, (7), 871-4.
9. Witlox, H. W. M., *Flashing Liquid Lets and two-Phase Dispersion, A Review, Det Norske Veritas Ltd., HSE Books, 2002.*
10. Perry, R. H.; Chilton, C. H.; Perry, J. H., *Chemical engineers' handbook.* 5th ed.; McGraw-Hill: New York,, 1973; p 1 v. (various pagings).
11. Kukkonen, J.; Kulmala, M.; Nikmo, J.; Vesala, T.; Webber, D. M.; Wren, T., The homogeneous equilibrium approximation in models of aerosol cloud dispersion. *Atmos. Environ. FIELD Full Journal Title:Atmospheric Environment* **1994,** 28, (17), 2763-76.
12. J. J. Martin and D. M. Longpre, New Property Tables of Chlorine in SI Units, Journal of Chemical and Engineering Data, Vol. 29, No. 4, pp. 468-473, 1984.
13. NTSB, *Collision of Union Pacific Railroad Train MHOTU-23 With BNSF Railway Company Train MEAP-TUL-126-D With Subsequent Derailment and Hazardous Materials Release, Macdona, Texas, June 28, 2004*, Railroad Accident Report, NTSB/RAR-06/03, National Transportation Safety Board, Washington, DC. **2006**.
14. NTSB, *Collision of Norfolk Southern Freight Train 192 With Standing Norfolk Southern Local Train P22 With Subsequent Hazardous Materials Release at Graniteville, South Carolina January 6, 2005*, Railroad Accident Report, NTSB/RAR-05/04, National Transportation Safety Board, Washington, DC. **2005**.
15. Joseph, G., Chlorine transfer hose failure. *J Hazard Mater* **2004,** 115, (1-3), 119-25.
16. CSB, *Investigation Report: Chlorine Release, DCP Enterprises, Festus, MO, August 14, 2002*, Report No. 2002-04-I-MO, U.S. Chemical Safety and Hazard Investigation Board. **May 2003**.
17. Routley, G. J., *Massive Leak of Liquified Chlorine Gas Henderson, Nevada (May 6, 1991)*, Report Number TR-052, Federal Emergency Management Agency, United States Fire Administration. **1991**.
18. McQuaid, J.; Roebuck, B. *Large scale field trials on dense vapor dispersion*; Res. Lab. Serv. Div.,Saf. Eng. Lab.,Sheffield,UK.: 1985; p 417 pp.
19. Ermak, D. L.; Chapman, R.; Goldwire, H. C.; Gouveia, F. J.; Rodean, H. C. *Heavy Gas Dispersion Test Summary Report*; Lawrence Livermore Natl. Lab.,Livermore,CA,USA.: 1989; p 169 pp.

20. Hanna, S. R.; Chang, J. C.; Strimaitis, D. G., Hazardous gas model evaluation with field observations. *Atmos. Environ., Part A FIELD Full Journal Title:Atmospheric Environment, Part A: General Topics* **1993,** 27A, (15), 2265-85.
21. Ermak, D. L.; Chan, S. T.; Morgan, D. L.; Morris, L. K., A comparison of dense gas dispersion model simulations with Burro series LNG spill test results. *J. Hazard. Mater. FIELD Full Journal Title:Journal of Hazardous Materials* **1982,** 6, (1-2), 129-60.
22. Spicer, T. O.; Havens, J. A., Field test validation of the DEGADIS model. *J. Hazard. Mater. FIELD Full Journal Title:Journal of Hazardous Materials* **1987,** 16, 231-45.
23. Puttock, J. S.; Colenbrander, G. W.; Blackmore, D. R., Maplin Sands experiments 1980: dispersion results from continuous releases of refrigerated liquid propane. *Heavy Gas Risk Assess.--2, Proc. Symp., 2nd FIELD Full Journal Title:* **1983**, 147-61.
24. Colenbrander, G. W.; Puttock, J. S., Maplin Sands experiments 1980: interpretation and modeling of liquefied gas spills onto the sea. *Atmos. Dispersion Heavy Gases Small Part., Symp. FIELD Full Journal Title:* **1984**, 277-95.
25. Brighton, P. W. M., Area-averaged concentrations, height-scales and mass balances. *J. Hazard. Mater. FIELD Full Journal Title:Journal of Hazardous Materials* **1985,** 11, 189-208.
26. Post, L.; Witlox, H.; McFarlane, K.; Roberts, P.; Hanna, S. R.; Chang, J. C.; Zhang, J. X., HGSYSTEM 3.0: Technical Reference Manual and User's Guide. **1995**.
27. EPA, *A Dispersion Model for Elevated Dense Gas Jet Chemical Releases, Volume 1*, EPA-450/4-88-006a, US Environmental Protection Agency, Research Triangle Park, North Carolina. **1988**.
28. EPA, *A Dispersion Model for Elevated Dense Gas Jet Chemical Releases, Volume 2: Users Guide*, EPA-450/4-88-006b, US Environmental Protection Agency, Research Triangle Park, North Carolina. **1988**.
29. Briggs, G. A.; Britter, R. E.; Hanna, S. R.; Havens, J. A.; Robins, A. G.; Snyder, W. H., Dense gas vertical diffusion over rough surfaces: results of wind-tunnel studies. *Atmos. Environ. FIELD Full Journal Title:Atmospheric Environment* **2001,** 35, (13), 2265-2284.
30. Giauque, W. F.; Powell, T. M., Chlorine: The Heat Capacity, Vapor Pressure, Heats of Fusion, and Vaporization and Entropy. **1939,** Vol. 61.
31. CRC handbook of chemistry and physics. In Chapman and Hall/CRCnetBASE: Boca Raton, FL, 1999; pp CD-ROMs.

6.0 NOMENCLATURE

Nomenclature

Symbol	Expanded Definition
A	vertical wind profile exponent
A	cloud top area
B	entrainment factor
C	cloud concentration
C_1	cloud concentration at the end of stage 1
C_D	orifice discharge coefficient
C_f	cloud concentration after aerosol evaporation
$C_{p,air}$	heat capacity of air
$C_{pL,H2O}$	heat capacity of liquid water
$C_{pL,TIC}$	liquid heat capacity
$C_{pS,H2O}$	heat capacity of ice
$C_{pV,TIC}$	vapor heat capacity
$C_{pV,H2O}$	specific heat of water vapor
d	hole diameter
D_c	cloud diameter
E	volumetric air entrainment ratio
f	friction factor
f_c	cloud height fraction when Richardson number equals 12
F_{H2O}	mass fraction of water in ambient air
F_J	vapor mass fraction in jet
f_v	vapor mass flux
F_{wv}	water vapor fraction remaining at final cloud temperature
g	gravitational acceleration constant
H_c	cloud thickness
H_d	total enthalpy before depressurization

Nomenclature (cont.)

Symbol	Expanded Definition
H_L	liquid enthalpy at boiling temperature
H_{Ld}	liquid enthalpy before depressurization
H_{tank}	total enthalpy after auto-refrigeration
H_{TIC}	liquid enthalpy at 20 C
H_V	vapor enthalpy at boiling temperature
H_{Vd}	vapor enthalpy before depressurization
L	hole length
M_1	chemical mass at the end of stage 1
M_2	chemical mass at the end of stage 2
$M_{air,dry}$	entrained dry air mass
M_c	total cloud mass
M_{H2O}	entrained water mass
M_{hs}	head space vapor mass
M_L	liquid mass in cloud
M_{L1}	chlorine liquid mass at the end of stage 1
M_{Ld}	liquid mass in tank before depressurization
M_R	recovered liquid mass
M_{tank}	initial mass
M_{TIC}	total chemical mass released
M_V	vapor mass in cloud
M_{Vc}	vapor leaving the tank
M_{Vd}	vapor mass in tank before depressurization
M_{VE}	cloud aerosol mass vaporized
P_{atm}	ambient air pressure

Nomenclature (cont.)

Symbol	Expanded Definition
$P_{s,H2O}$	saturation pressure of water at 20 C
$P_{s,ice}$	saturation pressure of ice at final cloud temperature
P_{tank}	tank pressure
$P_{s,TIC}$	chemical saturation pressure
P_V	partial pressure of chlorine vapor in cloud
Q	jet mass flow rate
Q_{ent}	average entrainment rate
Q_v	mass entrainment rate
Q_{v1}	average mass entrainment rate for stage 1
Q_{v2}	average mass entrainment rate for stage 2
Q_{v3a}	average mass entrainment rate for stage 3, part 1
Q_{v3b}	average mass entrainment rate for stage 3, part 2
Q_{vf}	mass entrainment rate after aerosol evaporation
R	ideal gas constant
Re	jet Reynold's number
RH	relative humidity
Ri_*	Richardson number
Ri_{*f}	Richardson number after aerosol evaporation
t	time from hole formation
t_2	duration of stage 2
t_{3a}	duration of stage 3, part 1
t_{3b}	duration of stage 3, part 2
T_{air}	ambient air temperature
T_b	chemical boiling temperature

Nomenclature (cont.)

Symbol	Expanded Definition
T_c	final cloud temperature
t_{ent}	entrainment duration
t_f	tank empty time
$T_{f,H2O}$	freezing temperature of water
T_{tank}	tank temperature
u_*	ambient air friction velocity
v	jet velocity
V_{air}	volume of air entrained
V_c	cloud volume
V_{H2O}	water vapor volume
V_{ice}	ice volume
V_L	chemical liquid volume
V_{tank}	tank volume
V_{TIC}	volume of chemical mass released
V_V	chemical vapor volume
w_*	vertical entrainment velocity
W_{air}	molecular weight of air
W_{H2O}	molecular weight of water
W_{TIC}	chemical molecular weight
α	mass evaporation ratio
$\Delta H_{f,H2O}$	heat of fusion of water
$\Delta H_{v,H2O}$	heat of vaporization of water
$\Delta H_{v,tank}$	heat of vaporization at 20 °C
$\Delta H_{v,TIC}$	chemical heat of vaporization at boiling temperature

Nomenclature (cont.)

Symbol	Expanded Definition
ΔP	pressure drop along hole length
ΔT	temperature decrease in tank
$\Delta U_{air,dry}$	energy change from cooling air
ΔU_{H2O}	energy change from cooling water vapor
ΔU_{ice}	energy change from forming and cooling ice
ΔU_{L}	energy change from cooling chemical liquid
ΔU_{V}	energy change from cooling chemical vapor
μ_{TIC}	liquid viscosity of chlorine
ρ_{air}	ambient air density
$\rho_{air,dry}$	partial density of dry air
ρ_{c}	cloud density with entrained air
ρ_{c1}	cloud density at the end of stage 1
ρ_{cf}	cloud density after aerosol evaporation
ρ_{cL}	liquid density at final cloud temperature
ρ_{H2O}	partial density of water vapor
ρ_{ice}	density of ice
ρ_{J}	density of jet at boiling temperature
ρ_{L}	liquid density at boiling temperature
ρ_{Ld}	liquid density depressurization
$\rho_{L,tank}$	liquid density in the tank
ρ_{tank}	fluid density in the tank
ρ_{V}	vapor density at boiling temperature
ρ_{Vd}	vapor density before depressurization

This page intentionally left blank.